International Journal of Hydrogen Energy 89 (2024) 634–647

Contents lists available at ScienceDirect

International Journal of Hydrogen Energy

journal homepage: www.elsevier.com/locate/he

Self-adaptive digital twin of fuel cell for remaining useful lifetime prediction

Ming Zhang, Amirpiran Amiri *, Yuchun Xu, Lucy Bastin, Tony Clark

College of Engineering and Physical Sciences, Aston University, Birmingham, B4 7ET, UK

ARTICLE INFO

Keywords:
Digital twins
Degradation prediction
Useful lifetime
Fuel cells
Transfer learning

ABSTRACT

Accurate prediction of the remaining useful life (RUL) of proton exchange membrane fuel cells (PEMFCs) is essential for maximizing their operational lifespan. However, existing methods often face limitations in two key areas: long-term prediction (beyond 168 h, or one week) and adaptability to varying operating conditions. To address these challenges, we propose a novel self-adaptive digital twin (SADT) model for RUL prediction of PEMFCs. Our approach uniquely integrates a deep convolutional neural network to generate robust health indicators (HIs) that maintain consistent monotonicity across diverse operating conditions. Additionally, we introduce a novel quantile Huber loss (QH-loss) function to enhance prediction accuracy and incorporate a transfer learning technique to improve adaptability under varying operational scenarios. Experimental results on PEMFC degradation datasets demonstrate that our method outperforms state-of-the-art techniques in long-term prediction accuracy, highlighting its potential to significantly extend fuel cell lifetimes.

1. Introduction

As one of the most efficient hydrogen utilization technologies, commercial fuel cells (FC) represent a promising avenue to realize the Net-Zero ambition, significantly contributing to the decarbonization of industries and the transportation sector [1]. Among these technologies, the Proton Exchange Membrane Fuel Cell (PEMFC) currently stands as the forefront choice for harnessing hydrogen in various transport modes, including buses, trains, and heavy goods vehicles (HGVs) [2]. Nowadays, the durability concern surrounding PEMFC systems has garnered increasing attention, emerging as a prominent obstacle to the widespread adoption of fuel cells in practical applications [3,4]. Hydrogen-based fuel cells inherently exhibit susceptibility to irreversible degradation due to their essential nature, ultimately leading to performance deterioration and a shortened operational lifespan [5]. Currently, over 27,000 hydrogen fuel cell battery electric vehicles (HFCBEVs) have been produced globally, with increasing numbers anticipated. In the UK, hundreds of hydrogen buses from WrightBus and Alexander Dennis are being ordered for cities like Birmingham, aiming to replace the 32,000 diesel buses in service by 2030 [6]. Such widespread adoption of fuel cell technology holds promise for achieving sustainable energy solutions and advancing the Net-Zero agenda. However, the durability and efficiency of PEMFCs currently fall short of the levels that will be crucial to support future commercial demands. In recent years, the average lifetime of PEMFCs has been approximately 2000 to 3000 h, but ongoing research aims to extend this to 6000 to 7000 h before 2030 [7].

Predictive maintenance (PdM) technology has undergone rapid development and has been integrated into the context of Industry 4.0. Its core objectives encompass the protection of critical assets, the extension of their operational lifespan, and the reduction of maintenance expenses [8–10]. Notably, this technology has also been harnessed for monitoring and accessing the state of health (SoH) of PEMFC systems and accurately predicting their remaining useful life (RUL) [7,11]. Equipped with precise degradation information, including SoH and RUL, operators can proactively schedule maintenance to avert unexpected failures. Therefore, the development of accurate and dynamic models to characterize degradation mechanisms, along with the exploration of precise, efficient, and resilient methods for RUL prediction, stand as critical challenges within the realm of PEMFC systems, particularly when confronting dynamic operating conditions.

The prediction of RUL for PEMFC systems has been a subject of extensive study spanning several years. This prediction process typically involves two essential steps: the construction of health indicators and the estimation of RUL. In the initial stages, researchers predominantly relied on model-based methods, notably employing techniques such as the Kalman filter and particle filter. However, models solely based on theoretical knowledge often struggle to provide accurate predictions aligned with real-world applications. Therefore, machine learning methods such as Artificial Neural Networks (ANN), Gaussian Process (GP), and Support Vector Machine (SVM) have been integrated with physics-based models to enhance prediction accuracy; these methods are generally known as hybrid model approaches. Across a range

* Corresponding author.
E-mail address: a.p.amiri@aston.ac.uk (A. Amiri).

https://doi.org/10.1016/j.ijhydene.2024.09.266
Received 27 June 2024; Received in revised form 8 September 2024; Accepted 19 September 2024
Available online 1 October 2024

of domains, purely data-driven approaches have garnered increasing attention in recent years, propelled by advancements in computing power and AI algorithms, including deep learning and evolutionary algorithms. The advantage of data-driven methods lies in their ability to construct prediction models using practical data from real-world applications, without relying on physical knowledge. Therefore, these approaches are of significant interest for PEMFC RUL prediction, reducing the complexity of application and facilitating widespread adoption.

Existing methods primarily focus on enhancing the accuracy of degradation prediction under constant operating conditions and are predominantly suited for short-term forecasting. However, these solutions often lack the capability to effectively support PEMFC RUL prediction in real-world applications. To meet the requirements of real-world applications, prediction models should demonstrate greater adaptability and higher prediction accuracy under various operating conditions. Additionally, long-term forecasting is essential for improved predictive maintenance and health management. To tackle these challenges, we propose a transfer learning enabled Self-Adaptive Digital Twin (SADT) for PEMFC, aimed at accurately predicting the Remaining Useful Life under both stable and dynamic operating conditions for long-term forecasting. Our approach integrates deep transfer learning techniques to improve adaptability and establish uniform State of Health labels for consistent long-term predictions. A significant innovation is the development of a novel loss function for SADT model training, combining the quantile Huber loss function with domain discrepancy regulation components. The proposed SADT solution promises to revolutionize PEMFC RUL prediction. Its integration of transfer learning techniques and novel loss functions enhances accuracy, adaptability, and understanding of fuel cell degradation mechanisms, paving the way for more reliable predictive maintenance strategies in diverse real-world applications.

2. Related work

2.1. Model-based methods

In the early stages of predicting the Remaining Useful Life (RUL) of PEMFCs, researchers focused on combining physical-based degradation models with filtering methods, such as the Kalman filter and particle filter. Chen et al. [12] proposed the combination of three empirical voltage models with the Unscented Kalman Filter to predict the FC prediction. Ao et al. [13] introduced the use of the frequency-domain Kalman filter (FDKF) and voltage degradation model to predict the degradation of PEMFCs in the frequency domain. Zhang et al. [14] improved prognostic performance by comparing it with a classical particle filtering-based approach. Wang et al. [15] integrated a novel degradation model with a particle filter to propose a model-based method for estimating the SOH, predicting the future degradation trend (FDT), and determining the remaining useful life (RUL) of PEMFCs.

As highly effective statistical tools, machine learning methods have been incorporated to construct and enhance prognostic degradation models. Liu et al. [16] utilized Adaptive Neuro-Fuzzy Inference Systems (ANFIS) and Particle Swarm Optimization (PSO) to enhance the semi-empirical voltage degradation model, enabling long-term RUL prediction. To enhance prognostic accuracy, Ma et al. [17] introduced a data-fusion approach for forecasting fuel cell performance. This approach combines Long Short-Term Memory (LSTM) with the Auto-Regressive Integrated Moving Average (ARIMA) method. Ma et al. [18] introduced a hybrid prognostic method that combines the extended Kalman filter (EKF) and Long Short-Term Memory (LSTM) recurrent neural network. The EKF is employed to estimate three parameters based on the output voltage, followed by the use of the data-driven LSTM method to predict voltage. Zuo et al. [19] constructed a single-cell test rig with voltage output. They explored the performance of four different neural network structures, including Gated Recurrent Unit (GRU), Attention-based Long Short-Term Memory (LSTM), and Attention-based GRU, for short-term voltage prediction. Yue et al. [20] introduced a method that combines degradation parameter extraction and Echo State Networks (ESN) to achieve long-term degradation prediction under dynamic operating conditions. Wang et al. [21] developed a modified degradation behavior model based on the polarization curve. They subsequently employed a symbolic-based LSTM prognostics model to predict the Health Indicator (HI) trend over the long term. The Gaussian process-related methods have been utilized to realize degradation prediction by Zhu et al. [22] and Deng et al. [23]. The short-term prediction of single-step-ahead voltage is estimated using datasets encompassing both constant and dynamic operational conditions.

2.2. Data-driven methods

Data-driven approaches differ from physics-based methods in that they are employed to establish highly nonlinear relationships between input signals and output predictions. Future states and RUL are estimated based on historical SoH trends, eliminating the need to construct physics-based models based on complex degradation mechanisms. In this context, it is not necessary to fully understand the various interactive degradation mechanisms that drive degradation at cell and stack scales. Instead, data-driven methods treat the degradation phenomena caused by different components as a whole. Data-driven approaches are typically employed in cases where fundamental modeling of the degradation process is challenging. The multi-input and multi-output Echo State Neural Network (MIMO-ESN) has been employed to construct HIs and further enhance prediction accuracy under various operational conditions [24–26]. Multiple operational parameters, such as current, temperature, and pressure, serve as inputs to the ESN-based model, and the prognostic models have been validated for long-term predictions [27,28]. The Long Short-Term Memory (LSTM) network is an enhanced version of the Recurrent Neural Network (RNN), specifically designed to address issues related to gradient exploding and vanishing. LSTM has been incorporated into the prediction of PEMFC system degradation under dynamic working conditions, primarily for short-term predictions [29–31]. Chen et al. [32] proposed the use of evolutionary algorithms, including the Memetic Evolutionary Algorithm (MEA), Particle Swarm Optimization (PSO), and Genetic Algorithm (GA), in conjunction with a Backpropagation Neural Network to construct an aging prognosis model for PEMFC. Yang et al. [33] employed the Improved Grey Wolf Optimizer (IGWO) and the Backpropagation (BP) neural network to predict the RUL of a vehicle-oriented PEMFC system. These evolutionary algorithms are applied to optimize the parameters of the constructed prognostic model. Mezzi et al. [34] proposed the combination of Echo State Networks (ESN) and Markov chains to predict degradation under variable load profiles. This approach yielded satisfactory results without the need for complicated data processing. However, it is important to note that the predictions are still made under short-term circumstances. Hua et al. [35] proposed a data-driven approach called Discrete Wavelet Transform-Echo State Network-Genetic Algorithm (DWT-ESN-GA) to enhance RUL prediction performance. Initially, historical datasets are compressed using DWT. Subsequently, the approximation components of the original data, including voltage and current, are predicted in the compressed space using ESN. It is worth noting that this approach is capable of deploying long-term RUL prediction.

2.3. Research gaps

The literature review reveals two major research gaps in predicting RUL of fuel cells. First, there is a lack of well-established methods for constructing general HIs. Traditional static HIs are inadequate for various working conditions due to the varying uncertainty of load and current. An effective HI for the PEMFC system should be easy to

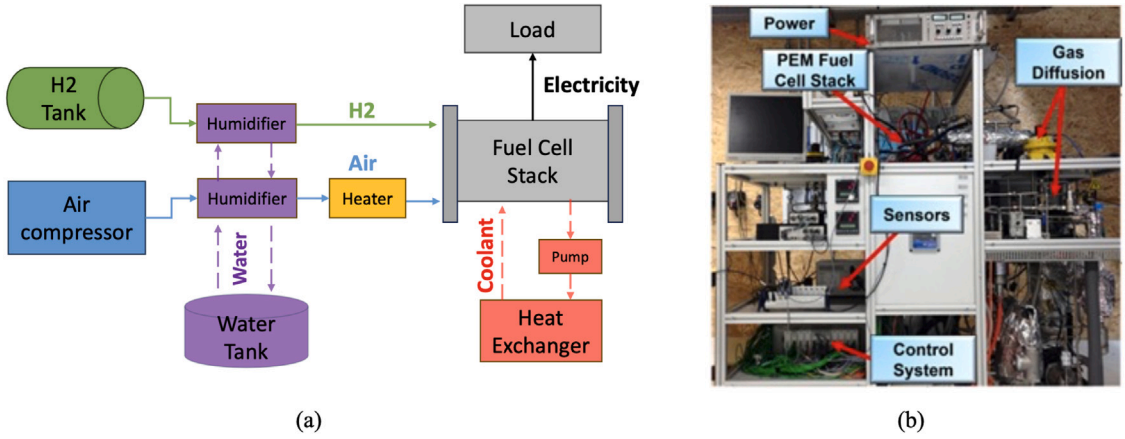

Fig. 1. (a) Schematic of a typical PEM fuel cell system; (b) PEMFC test rig.

deploy, exhibit a generally monotonic trend over time, and be applicable to various operational states. Secondly, the prediction processes of existing methods are often time-consuming and heavily reliant on expert intervention. This limits their applicability to laboratory and offline analyses, preventing them from being implemented for real-time predictions in practical scenarios with dynamic conditions or the management of multiple fuel cells.

Therefore, we propose a transfer learning-enabled self-adaptive digital twin of a fuel cell to predict the remaining useful lifetime of PEMFC, addressing these research gaps. First, we employ a powerful deep convolutional neural network to construct the prognostic model capable of predicting dimensionless HIs that exhibit a generally monotonic trend with time and are effective across different working conditions. Next, transfer learning is employed to enable self-adaptation when the prognostic model handles real-time raw data under varying working conditions.

3. Preliminary

3.1. Polymer electrolyte membrane fuel cells (PEMFC) system

The PEMFC is a cutting-edge electrochemical device that generates electrical energy through the direct conversion of hydrogen and oxygen into water, producing electricity and heat as byproducts. As depicted in Fig. 1 (a), a fuel cell system comprises the stack, serving as the core of the entire system, and is associated with various components, including a heat exchanger, air compressor, hydrogen tank, cooling system, humidifier, etc. At the start of the process, the hydrogen fuel is fed to the anode side of the fuel cell stack, while the oxidant (air) is delivered to the cathode. The compressor regulates the air mass flow at the cathode input and maintains pressure at the output. A humidifier is integrated into the system to introduce water content to the air—an essential step in operating the fuel cell and preventing damage to the membranes caused by drying out. The cooling system, consisting of a heat exchanger and pump, is employed to maintain a stable temperature within the fuel cell.

A real PEMFC test rig, built by the FCLAB Research Federation [36], is illustrated in Fig. 1 (b). All operating parameters within the control system are detailed in Table 1. Both the hydrogen and air pass through separate humidifiers. The air is pre-heated to reach the operating temperature, while the hydrogen remains at room temperature. To regulate the stack temperature, a heat exchanger system is utilized. The current supplied by the battery is regulated by a TDI Dynaload active load.

3.2. Remaining useful life prediction for PEMFC

RUL prediction is a vital aspect of predictive maintenance, providing an estimate of the remaining time that a system or component will operate before reaching the end of its useful life. The principles of RUL prediction are depicted in Fig. 2. RUL is defined as the duration between the current instant t_i and the point t_{EOF} at which the system reaches the failure threshold at the end of its life (EOL). The initial step involves extracting degradation features from available measurements. Subsequently, a prognostic method is designed to forecast future information in the absence of real-time measurements. The prediction is executed through a training process with the goal of determining the RUL value based on the specified EOL threshold.

Table 1
PEMFC operating parameters.

Parameter types	Value range
Temperature range for cooling (°C)	20–80
Cooling flow (l/min)	0–10
Gas temperature (°C)	20–80
Gas humidification %RH	0–100
Airflow (l/min)	0–100
Flow of fuel (l/min)	0–30
Gas pressure (bars)	0–2 bars
Fuel cell current (A)	0–300

The majority of existing RUL prediction methods for PEMFCs focus on short-term forecasts, typically less than 24 h (1 day) [3]. Given the PEMFC's lifespan of thousands of hours, such short-term predictions may not allow sufficient time for proactive maintenance actions. In practice, long-term degradation predictions are more beneficial for effective maintenance and management strategies. To facilitate long-term prediction for PEMFCs and adhere to the principles of RUL prediction, we establish a mathematical specification outlining the RUL prediction for PEMFCs, along with associated measurement properties, which is shown in Fig. 3. At any time i, the measurement x_i comprises temperature $Temperature_i$, pressure $Pressure_i$, flow rate $Flowrate_i$, humidity $Humidity_i$, current $Current_i$, and voltage $Voltage_i$. The state of health y_i is determined using the evaluation function F_{eval}. The prediction function F_{pred} is learned from the historical dataset $[(t_0, y_0), (t_1, y_1), \ldots, (t_i, y_i)]$. The end-of-life time t_{EOF} is calculated directly using the state of health threshold y_{thre}. Finally, the RUL value is obtained as $t_{EOF} - t_i$.

4. Method

4.1. Self-adaptive digital twin (SADT) architecture

The self-adaptive digital twin, empowered by the transfer learning method, is proposed in this work for predicting the remaining useful life of PEMFC. This innovative approach effectively leverages pre-existing knowledge and data, enabling the digital twin to autonomously adapt

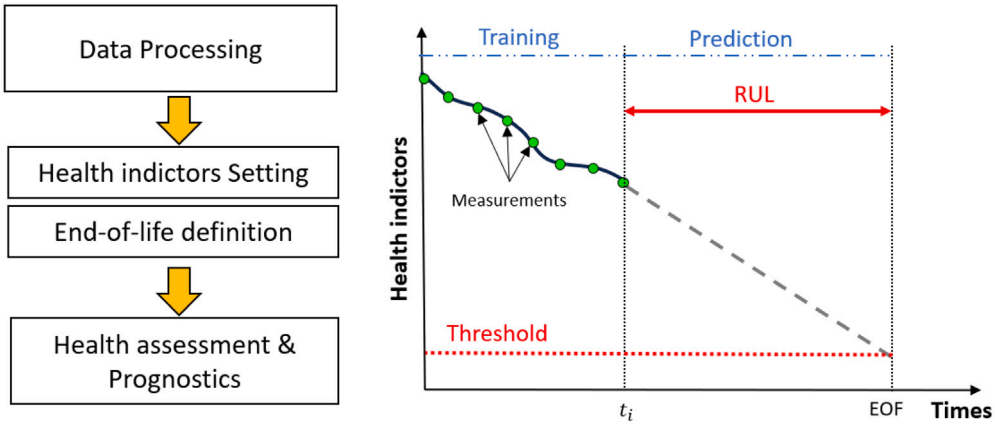

Fig. 2. Principles of Remaining Useful Life Prediction.

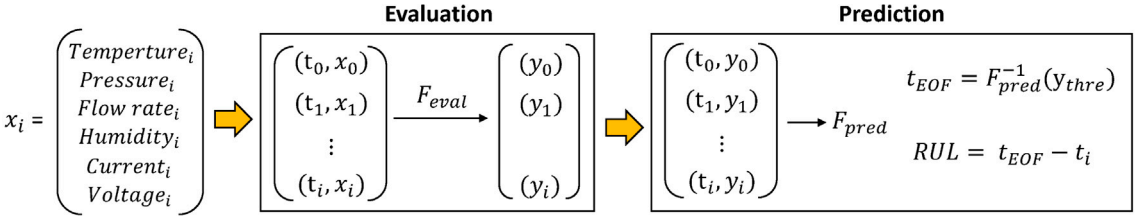

Fig. 3. Mathematical specification for long-term RUL predicting of PEMFC.

and refine its parameters for accurate and real-time predictions across varying working conditions. The Self-Adaptive Digital Twin (SADT) architecture, as shown in Fig. 4, integrates both historical and real-time data for predicting the RUL of PEMFCs. The process begins with offline supervised learning, where historical labeled data is used to train a prognostic model. Subsequently, a replica of the trained model is deployed on-site to predict the health state, while it automatically adapts to new operating conditions using transfer learning. The self-adaptive mechanism continuously updates the model with real-time operational data from the PEMFC. This updated prognostic model then assesses the current SoH and provides an accurate prediction of the RUL. This architecture ensures that the model remains adaptable and accurate under changing operating conditions, enhancing its reliability for long-term predictions.

4.2. Implementation with deep transfer learning framework

In this paper, we propose a deep transfer learning (TL) framework to implement the SADT for RUL prediction of PEMFC. The TL framework is illustrated in Fig. 5. The process involves two critical steps: offline training, which entails supervised learning using raw data and labels from the source domain, and online adaptation, where the model undergoes domain adaptation using raw data from the target domain. In our TL framework, we utilize a deep convolutional neural network to predict the SoH labels. The domain adaptation method is employed to enhance adaptability across different operating conditions. Additionally, we introduce a novel quantile Huber loss (QH-loss) to improve prediction accuracy.

4.2.1. Convolutional neural network

A deep Convolutional Neural Network (DCNN) is a highly effective deep learning architecture specifically designed for processing image and sequence data [37–39]. This model has significantly advanced computer vision by autonomously extracting meaningful features from input data using convolutional layers. Comprising convolutional, pooling, and fully connected layers, CNNs learn parameters through backpropagation during training [40]. Their ability to capture intricate patterns has led to remarkable success, solidifying CNNs as a fundamental component of modern machine learning."

In the context of image classification, a standard convolutional layer comprises an input image represented as I and a kernel K. This layer conducts a two-dimensional convolution, defined as:

$$S(i,j) = (I * K)(i,j) = \sum_m \sum_n I(m,n)K(i-m, j-n) \tag{1}$$

In this paper, we utilize one-dimensional convolution in each convolutional layer. This simplification is accomplished by setting m to 1. The one-dimensional convolution can be expressed as:

$$C_{ij}^l = \phi(k^j n \times 1 * x_{i:i+n}^i + b_{ij}) \tag{2}$$

Here, $k_{n\times 1}^j$ represents the jth kernel belonging to the kernels K_j^l of size $n \times 1 \times j$ in the lth convolutional layer. $x_{i:i+n}^i$ denotes the ith input segment, bij corresponds to the bias, and ϕ represents the activation function, which can be Sigmoid, Tanh, Relu, or leakyRelu. C_{ij}^l signifies the ith feature point of the jth kernel in the lth convolutional layer.

The deep convolutional neural network (CNN) in our proposed SADT model plays a crucial role in predicting effective Health Indices (HIs) by learning and extracting features from the input data that are indicative of the fuel cell's health status. Specifically, the CNN is designed to manage the complexity of various working conditions and is trained to produce HIs that are consistent in range and monotonicity across different operating scenarios. The network achieves this through two key aspects: (1) Feature Extraction: The CNN automatically learns relevant features from raw sensor data through multiple layers of convolutions and pooling operations, helping to identify patterns indicative of the fuel cell's degradation. (2) Consistency: By training on a diverse set of operating conditions, the CNN ensures that the HIs produced have a uniform range and exhibit monotonic behavior, thereby enhancing their reliability for RUL prediction.

4.2.2. Domain adaption method

The domain adaptation method has been chosen to facilitate the online adaptation process. For domain adaptation, we have a source domain $D_s = \{x_i^s, y_i^s\}_{i=1}^{n_s}$ containing n_s labeled data samples and a

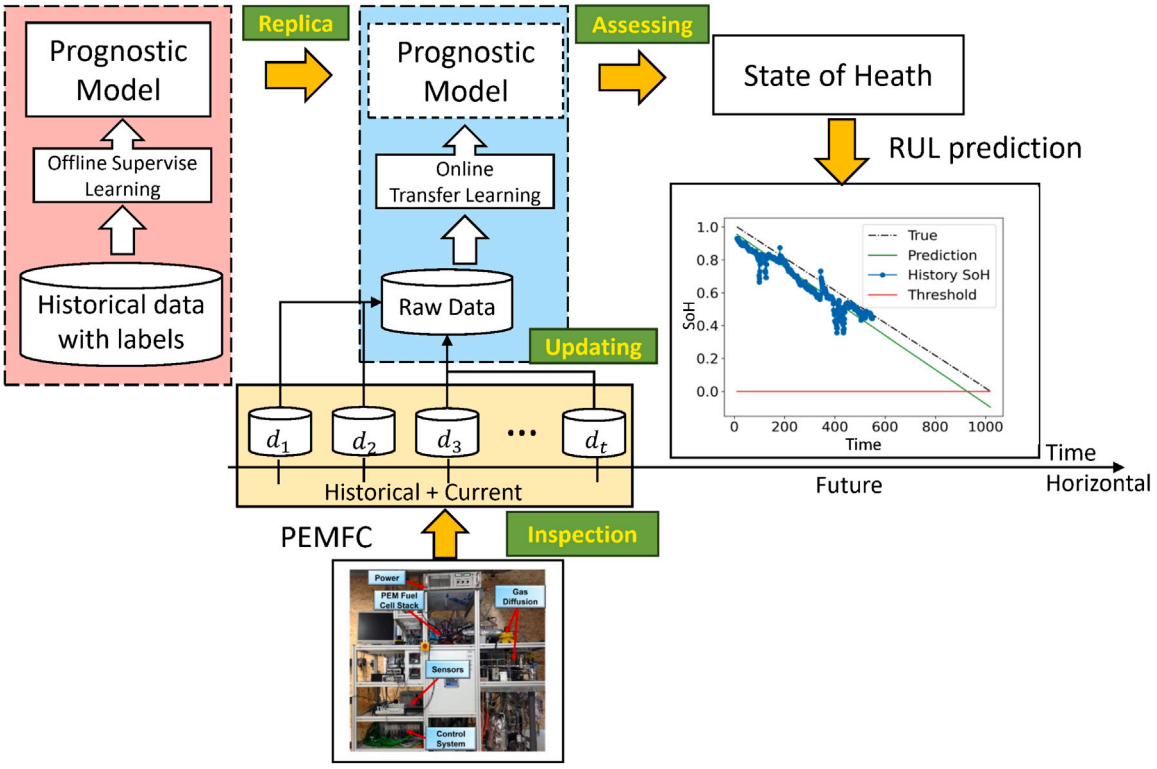

Fig. 4. Self-Adaptive Digital Twin (SADT) Architecture.

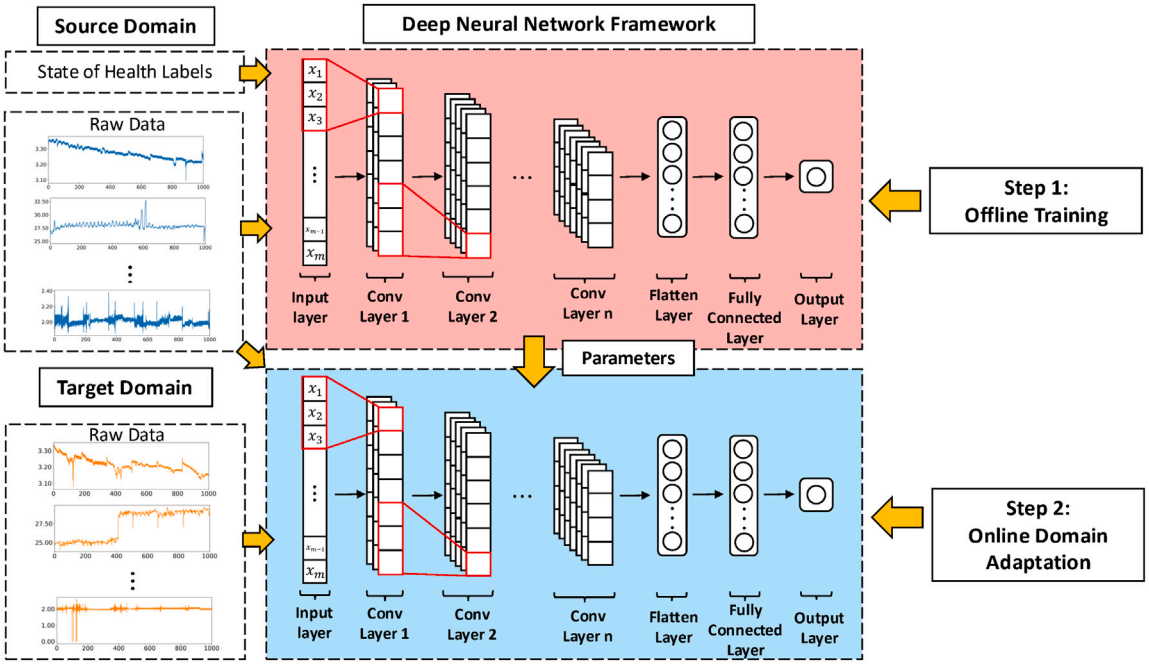

Fig. 5. The architecture of deep neural network with domain adaptation.

target domain $D_t = \{x_j^t\}_{j=1}^{n_t}$ consisting of n_t unlabeled data samples. These domains are characterized by probability distributions p and q, respectively. The goal is to develop a deep neural network capable of learning transferable features that address the cross-domain discrepancy. Ultimately, our objective is to construct a predictor $y = \theta(x)$ that minimizes the target risk $\epsilon_t(\theta) = Pr_{(x,y)\sim q}[\theta(x) \neq y]$ for the target domain.

In this study, we adopt the multiple kernel variant of maximum mean discrepancies (MK-MMD) [41] to mitigate the discrepancy between the source and target domains. MK-MMD between two distributions, p and q, is characterized by the distance between their embeddings in the Reproducing Kernel Hilbert Space (RKHS), denoted as $\mathcal{H}_k$. This can be formulated as:

$$d_k^2(p,q) \triangleq \|E_p[\phi(x^s)] - E_q[\phi(x^t)]\|_{\mathcal{H}_k}^2. \quad (3)$$

Here, the kernel function $k(x^s, x^t) = \langle \phi(x^s), \phi(x^t) \rangle$ is constructed using a feature map ϕ, which represents a convex combination of m positive semi-definite (PSD) kernels, denoted as k_u:

$$\mathcal{K} \triangleq \{k = \sum_{u=1}^{m} \beta_u k_u : \sum_{u=1}^{m} \beta_u = 1, \beta_u \geq 0, \forall u\}, \tag{4}$$

The constraints imposed on the coefficients β_u guarantee the characteristic nature of the resulting multi-kernel k.

As a transfer learning technique, the domain adaptation algorithm is employed to address the challenge of transferring knowledge from one operating condition (source domain) to another (target domain) where conditions differ. In our study, this method is critical for enhancing the prediction accuracy and adaptability of our model across various operating conditions, ranging from constant working conditions to quasi-steady states. The domain adaptation technique improves prediction adaptability through the following mechanisms: (1) Feature Alignment: It aligns the feature distributions of the source and target domains, helping to mitigate discrepancies between different operating conditions. By minimizing the distribution shift, the model can generalize more effectively from one domain to another. (2) Adaptive Learning: The method adjusts the model parameters to accommodate variations in operating conditions, allowing the model to learn from target domain data more effectively and improving its performance in predicting the HIs under diverse conditions.

4.2.3. Quantile Huber loss

A new quantile Huber loss (QH-loss) has demonstrated superior performance within the deep learning framework when compared to traditional mean square error (MSE) and mean absolute error (MAE) for general RUL prediction problems [42]. Therefore, we have opted to incorporate the QH-loss into our proposed SADT framework to enhance prediction accuracy for both source and target domain data.

To satisfy the QH-loss criteria, we build the cumulative distribution function (CDF) of the target distribution $F_Z(z|y^s)$ by employing the Gaussian distribution function with the true value y^s, expressed as follows:

$$F_Z(z|y^s, \sigma) = \frac{1}{\sigma\sqrt{2\pi}} \int_{-\infty}^{z} exp(-\frac{(t-y^s)^2}{2\sigma^2})\, dt. \tag{5}$$

The QH-loss, denoted as L_{QH}, is subsequently defined as follows:

$$L_{QH}(X^s, Y^s) = \sum_{i=1}^{N} \mathbb{E}[\rho_{\hat{\tau}_i}^{\kappa}(F_Z^{-1}(\hat{\tau}_i) - P(M(\hat{\tau}_i|x^s)))], \tag{6}$$

Here, M signifies a mapping layer comprised of multiple CNN layers, while P denotes a predictor composed of fully connected layers. The output of the quantile distribution at each quantile $\hat{\tau}_i$ is determined as $P(M(\hat{\tau}_i|x))$.

4.2.4. SoH labeling and RUL estimation

In order to facilitate RUL prediction across diverse operating conditions, we introduce the uniform labeling method in this study, depicted in Fig. 6. Given the significant variations in the true remaining lifetime associated with different working conditions, adopting uniform SoH labeling ranging from 1 to 0 emerges as the most effective strategy for enabling prediction across distinct domains. The expected SoH labeling should be a linear monotonic function, which will help the model anticipate the likely EoL. In this work, the deep CNN and the QH-loss function have been firstly introduced to map the fuel cell raw data to a simple linear health index, which is meaningful for maintenance planning across different operating conditions. Subsequently, the RUL value can be easily estimated using the least-square method, employing the basic function $R(t) = a - b \times t$, with the same EoL threshold set at SoH equal to 0. In this configuration, the proposed approach can autonomously implement RUL prediction across varying working conditions without requiring expert intervention.

In our study, the SoH refers to HIs, which are specific metrics or indicators derived from the fuel cell's operational data that reflect its health status and degradation level. These indices are estimated by a deep CNN model based on various operational parameters and serve as proxies for assessing the fuel cell's remaining useful life. The HIs mentioned in our paper are designed with three key aspects in mind: (1) Reflect Degradation: Capture and quantify the extent of degradation experienced by the fuel cell over time. (2) Ensure Uniformity: Maintain consistency in their numerical range and monotonic behavior, which is essential for accurate and reliable RUL prediction. (3) Support RUL Prediction: Provide a robust basis for predicting the remaining useful life of the fuel cell under different operating conditions.

4.2.5. Proposed SADT formulation

In our research, we optimize the SADT model on the source domain while simultaneously narrowing the distribution gap between the source and target domains to capture adaptable features at the fully connected layer. The unified loss function is outlined as follows:

$$\min_{\Theta} L_{QH}(X^s, Y^s) + \lambda d_k^2(D_s^l, D_t^l), \tag{7}$$

Here, $L_{QH}(X^s, Y^s)$ denotes the QH loss on the source domain, while $d_k^2(D_s^l, D_t^l)$ represents the squared MK-MMD discrepancy between the labeled source domain D_s^l and the unlabeled target domain D_t^l. The parameter $\lambda > 0$ serves as a penalty parameter regulating the trade-off between the two components of the loss function.

4.3. Workflow of the proposed method

The overall workflow of our proposed method is expressed as follows:

1. Offline training involves utilizing recorded source domain data comprising raw data and their labels, denoted as $D_s = \{x_i^s, y_i^s\}_{i=1}^{n_s}$, to train the SADT model. In this step, We employ the QH-loss, as depicted in equation (6), within a standard supervised learning strategy.
2. Online adaptation entails leveraging newly collected raw data in the target domain from the real-time monitoring system, represented as $D_t = \{x_j^t\}_{j=1}^{n_t}$, to fine-tune the SADT model. During this phase, we optimize the SADT model according to equation (7) using a domain adaptation strategy.
3. RUL prediction involves utilizing the predicted SoH labels of the target domain data, denoted as $\{\hat{y}_j^t\}_{j=1}^{n_t}$, and then employing the least-square method to estimate the RUL value.

5. Experiments

5.1. Data preparation

In this study, we utilized a dataset collected from a PEM fuel cell test rig by the FC lab research federation (see Fig. 1) [36]. The test rig has a maximum electrical power output of 1 kW. To operate the fuel cell stack effectively, various parameters must be carefully monitored and controlled, as outlined in Table 2. The air boiler is heated to achieve the desired humidity level, while the hydrogen boiler is maintained at room temperature. The temperature of the fuel cell stack is precisely regulated using a cooling system. The test rig incorporates five fuel cell stacks, each with a 100 cm^2 active area and a nominal current density of 0.7 A/cm^2. All the monitoring features, depicted in Table 2, serve as input variables for predicting the RUL of the fuel cell.

In this dataset, two long-term experiments were conducted. Fig. 7 (a) depicts the first stack, FC1, which operated under stationary conditions, closely approximating nominal operating conditions. Conversely, the second stack, FC2, underwent dynamic current testing with high-frequency current ripples, which is considered quasi-steady state. The degradation voltage profiles for both FC1 and FC2 are illustrated in

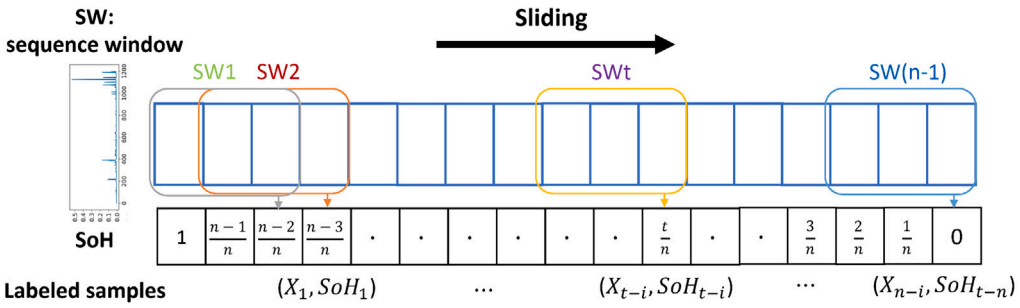

Fig. 6. Uniform SoH labeling method.

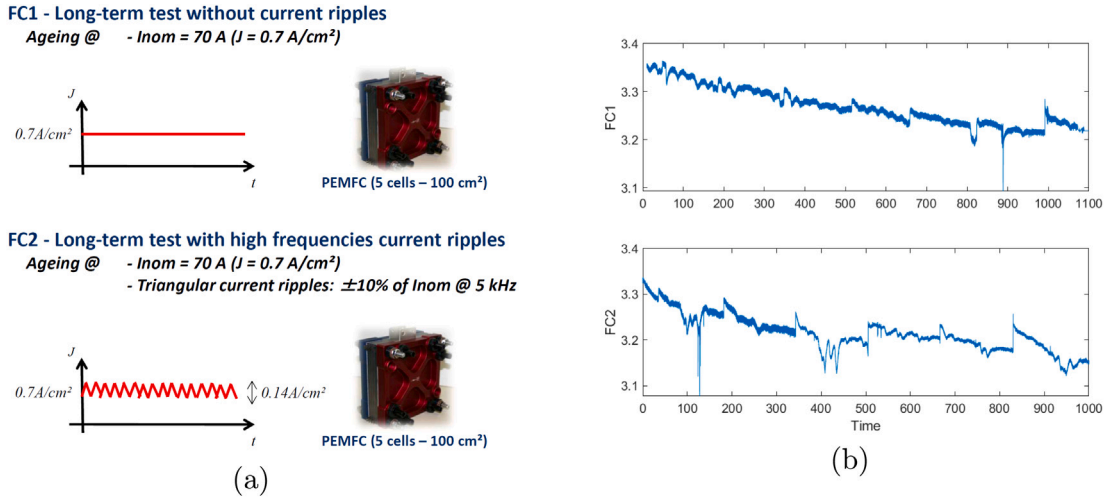

Fig. 7. (a) Durability tests performed for the challenge;(b) Raw data of Voltage of FC1 and FC2.

Table 2
Details of operating parameters.

Monitoring parameters	Physical meaning
Time	Aging time (h)
U1 to U5; Utot	Single cells and stack voltage (V)
I;J	Current (A) and current density (A/cm^2)
TinH2; ToutH2	Inlet and Outlet temperatures of H2 (°C)
TinAIR; ToutAIR	Inlet and Outlet temperatures of AIR (°C)
PinH2; PoutH2	Inlet and Outlet Pressure of H2 (mbara)
PinAIR ; PoutAIR	Inlet and Outlet Pressure of Air (mbara)
DinH2 ; DoutH2	Inlet and Outlet flow rate of H2 (l/mn)
DinAIR ; DoutAIR	Inlet and Outlet flow rate of Air (l/mn)
DWAT	Flow rate of cooling water (l/mn)
HrAIRFC	Inlet Hygrometry (Air) - estimated (%)

Table 3
Details of deep convolutional neural network structure.

Block	Layer type	Kernel	Stride	Channels	
				in	out
CNN layer 1	Convolution ReLU Max Pooling	5 × 1 2 × 1	1 × 1 2 × 1	1	32
CNN layer 2	Convolution ReLU Max Pooling	7 × 1 1 × 1	1 × 1 2 × 1	32	64
CNN layer 3	Convolution ReLU Max Pooling	11 × 1 2 × 1	1 × 1 2 × 1	64	128
FC layer 1	Linear ReLU			1152	512
FC layer 2	Linear ReLU			512	128
Output layer				128	1

Fig. 7 (b). The operating parameters of FC1 and FC2 throughout their lifespan are presented in Fig. 8. The majority of operating parameters remain consistent throughout the entire duration of the experiments for FC1 and FC2, with notable differences observed in current, current density, and the inlet temperatures of H2 and air. We attribute these variations to the differences between constant conditions and quasi-steady state.

5.2. Implementation details

The specifications of the proposed deep convolutional neural network are detailed in Table 3. Consistent with the approaches outlined in [43,44], our architecture incorporates three CNN layers and two fully connected layers utilizing ReLU activation functions. All the operational parameters, including current and voltage, listed in Table 2 are used as inputs to the deep CNN model, which outputs the linear and monotonic SoH labeling. All experiments were executed on a computer outfitted with an Nvidia GeForce GTX 4060 GPU, an Intel Core i9-13900HX CPU operating at 2.20 GHz, and 32 GB of memory. The default hyperparameter values are outlined in Table 4.

5.3. Measure indicators

This paper quantitatively assesses the prediction performance of the proposed method through three key metrics: mean absolute error (MAE), root mean square error (RMSE), and R^2 score. These metrics

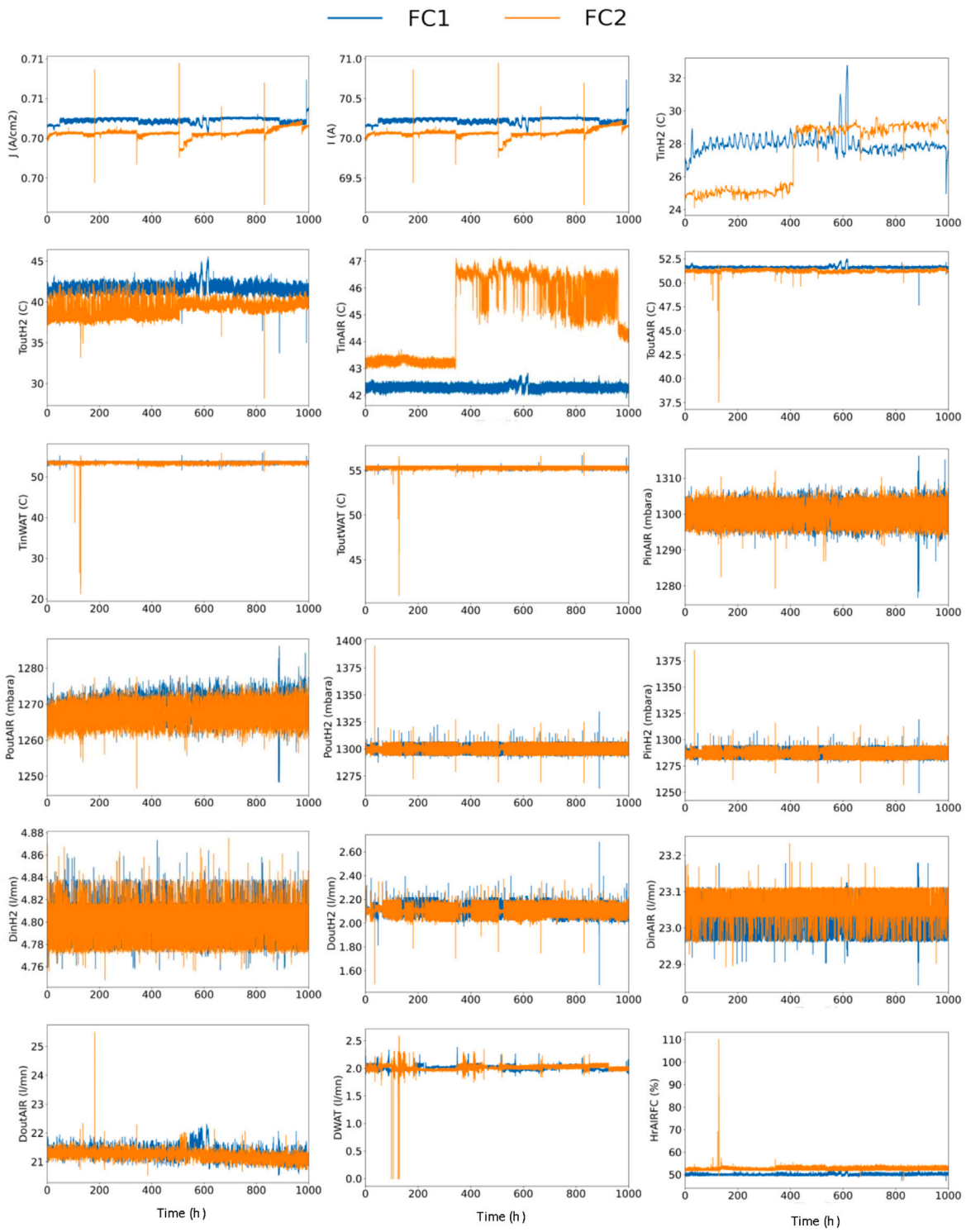

Fig. 8. Operating parameters of FC1 and FC2.

are defined as follows:

$$MAE = \frac{1}{Q}\sum_{i=1}^{Q}|\hat{y}_i - y_i| \tag{8}$$

$$RMSE = \sqrt{\frac{1}{Q}\sum_{i=1}^{Q}(\hat{y}_i - y_i)^2} \tag{9}$$

$$R^2 = 1 - \frac{\sum_{i=1}^{Q}(\hat{y}i - y_i)^2}{\sum_{i=1}^{Q}(\bar{y} - y_i)^2} \tag{10}$$

Here, Q denotes the total number of testing samples, $\hat{y}_i$ represents the predicted state of health (SoH) value, y_i signifies the true value of SoH (label), and $\bar{y}$ symbolizes the mean of all the true SoH values. Following the approach outlined in [9], we assess the RUL prediction results using the error Er_t, which is defined as:

$$Er_t = \frac{r_t - \hat{r}_t}{r_t} \times 100 \tag{11}$$

Here, variables r_t and $\hat{r}_t$ represent the actual and predicted RUL values, respectively.

Table 4
Default hyperparameters of the proposed method.

Hyperparameters	Value
Learning rate	0.001
Batch size	64
Pretrain epochs	20
TL epochs	100
QH-loss factor N_τ	5
QH-loss factor κ	1.0
QH-loss factor σ	0.2
Penalty λ	0.01

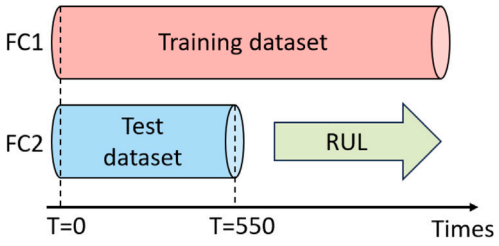

Fig. 9. Default FC RUL testing setting.

5.4. Result and analysis

5.4.1. RUL prediction

The default settings for fuel cell RUL prediction are described in [36]. As depicted in Fig. 7, two types of data are available for this challenge. The data from the experiment on FC1 is fully provided, referred to as the 'learning dataset'. In contrast, the data from the experiment on FC2 is only partially available, up to time $t = 550$ h, and is termed the 'testing dataset'. The default experiment settings are presented in Fig. 9. The challenge focuses on predicting the RUL, defined as the time until a specific level of power loss occurs. Specifically, we consider various power drop thresholds for FC1, such as $3.5\%, 4\%, 4.5\%, 5\%$, and 5.5% of the initial power (P_{init}). Subsequently, the challenge centers on FC2, where the goal is to predict the remaining time until a predefined time point, $t_{pred} = 550$ h.

The results of SoH evaluation and its subsequent prediction are presented in Fig. 10, highlighting the effectiveness of our proposed method. In these results, we adhere to the default prediction setting by assessing the SoH using the initial 550 h of data and then predicting RUL based on the evaluated SoH. The results shown in Fig. 10 illustrate the RUL prediction outcome for FC2 at 550 h with different failure thresholds set at 3.5%, 4.0%, 4.5%, 5.0%, and 5.5% of P_{init} based on the pre-trained model learned from the training data of FC1. The blue line represents the estimated SoH from 0 to 550 h, while the green line illustrates the learned function for predicting the RUL value. As described in our methodology, uniform SoH labels are employed. Therefore, the threshold for determining the EoL for both FC1 and FC2 is $SoH = 0$, indicated by the red line in Fig. 10. Comparing with the black dotted line, which represents the true label for FC2, the RUL prediction results are quite similar, with accuracy falling within an acceptable range. It is worth noting that our approach demonstrates robustness and adaptability to real-time data in the FC2 scenario, underscoring its potential for practical application.

The quantitative results of various measurement indicators are presented in Table 5, offering insight into the performance of the proposed method on FC2 under different failure thresholds of FC1. From these results, it is evident that the model performs optimally when considering a 4.5% power loss threshold (P_{init}). Additionally, the prediction results for other thresholds exhibit similar performance. This observation suggests that the performance of the adapted model on FC2 is not significantly influenced by the failure threshold of the FC1 training dataset. The results presented in Table 5 further validate the consistency of the findings depicted in Fig. 10.

5.4.2. Comparison with different start time

To further investigate the adaptability of our proposed method throughout the entire degradation period, we conducted tests on the digital model using different starting times. In the source domain, we set the failure threshold at 4.5% of P_{init} and utilized the complete dataset from FC1, including labels, for pre-training the digital model. Then, in the target domain, only raw data with varying prediction start times (ST) was available. The selection of the ST indicates the number of input data points from the target domain employed in the self-adaptation process of the pre-trained model to enhance predictions for the FC2 scenario. The results, as depicted in Fig. 11, highlight that the SoH assessment consistently performs well across different STs, achieving an R^2 value exceeding 0.85 throughout the entire period. Meanwhile, the RUL prediction performs well as the time approaches its EoL. Although the results are quite reasonable, indicating that more data collected for FC2 will lead to more accurate RUL predictions, it should be noted that our future work will focus on increasing the RUL prediction accuracy even in the very early stages of new adaptation scenarios.

5.4.3. Comparison with different loss function

To provide a more in-depth analysis of our proposed method, we conducted a comprehensive comparison between the QH-loss function and the traditional Mean Squared Error (MSE) and Mean Absolute Error (MAE) loss functions within the default prediction scenario. For this comparative analysis, we employed two key evaluation metrics: R^2 and Er, which assess performance independently of actual lifetime cycles. The results, showcased in Fig. 12, unequivocally demonstrate the superiority of the QH-loss when integrated into our proposed deep neural network structure. In terms of prediction accuracy and robustness, the QH-loss consistently outperforms both MSE and MAE. This compelling comparison underscores the exceptional performance of the QH-loss in this specific context, affirming its efficacy for accurate and reliable predictions.

5.4.4. Feature visualization

In order to further investigate the effectiveness of the proposed method, we have employed the T-SNE feature visualization method [45] to analyze the unlabeled raw data from the target domain. T-SNE is widely recognized for its effectiveness in compressing high-dimensional features from deep learning frameworks into two-dimensional visual images, allowing for easy validation of whether the deep model has been trained effectively or not. In this work, we selected data from a scenario where the failure threshold was set to $P_{init} = 4.5\%$ to demonstrate the performance before and after the online adaptation process. The visualization results are illustrated in Fig. 13. In this depiction, the color bar spans from 0 (red) to 100 (blue), effectively indicating the normalized ground truth SOH. To enhance visibility, a scaling factor of 100 has been applied. The mixed and irregular features shown in Fig. 13 (a) indicate that the SADT model cannot work effectively with this new data from dynamic operating conditions before adjustment. However, the effectiveness of the online self-adaptive approach has been validated with the visualization results shown in Fig. 13 (b), indicating well-trained models. Specifically, the features exhibit a regular transition from 100 to 0 without evident misclassification.

5.4.5. Comprehensive comparisons

To further validate the robustness of the proposed method, we conducted experiments by switching FC1 and FC2 as the source and target domains. In this scenario, FC2 was used as the source domain for training, and we then estimated the RUL values for FC1 at 550 h across different failure thresholds. The quantitative results are presented in Table 6. Notably, the 4.0% threshold yields the lowest error rate (Er = −3.6247) and the highest R^2 value (0.9817), indicating optimal accuracy at this threshold. When comparing these results with

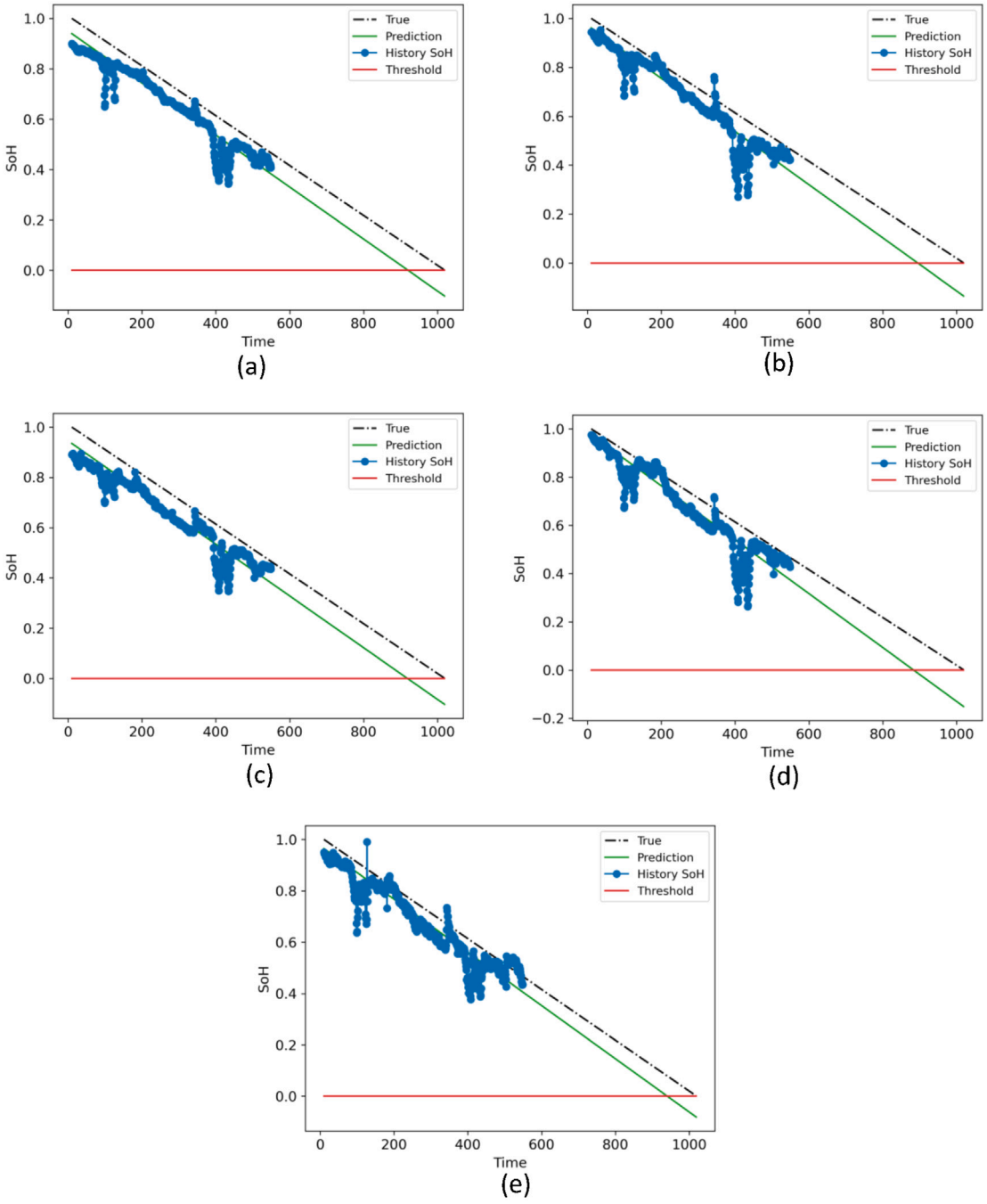

Fig. 10. RUL prediction results by SADT for FC2 at 550 h: (a) 3.5% of P_{init}, (b) 4.0% of P_{init}, (c) 4.5% of P_{init}, (d) 5.0% of P_{init}, (e) 5.5% of P_{init}.

Table 5
RUL prediction quantitative results by SADT for FC2 at 550 h.

t_{pred} = 550 h	Est RUL	Er	RMSE	MAE	R^2
Failure threshold: 3.5% of P_{init}	371	20.8955	0.0673	0.0523	0.9455
Failure threshold: 4.0% of P_{init}	346	26.2260	0.0654	0.0491	0.9485
Failure threshold: 4.5% of P_{init}	334	28.7846	0.0640	0.0432	0.9508
Failure threshold: 5.0% of P_{init}	369	21.3220	0.0722	0.0558	0.9374
Failure threshold: 5.5% of P_{init}	331	29.4243	0.0797	0.0616	0.9237

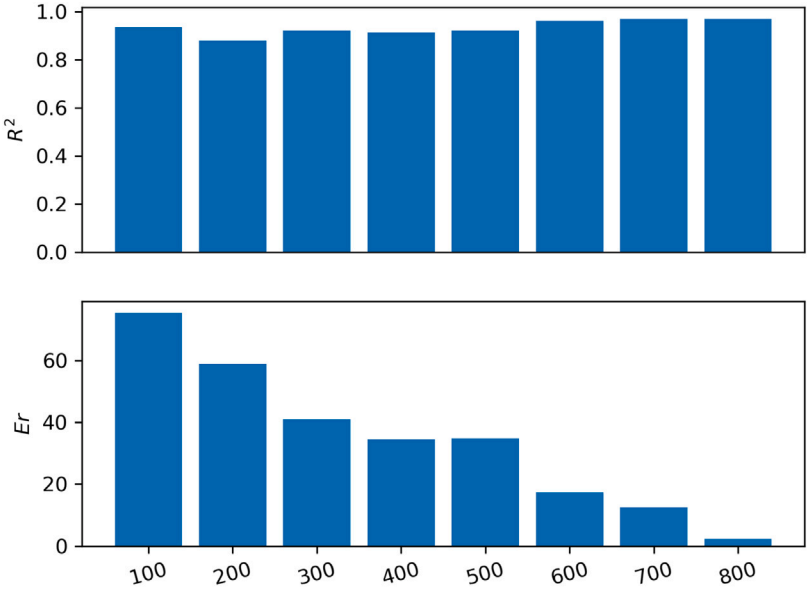

Fig. 11. Comparison with different start time.

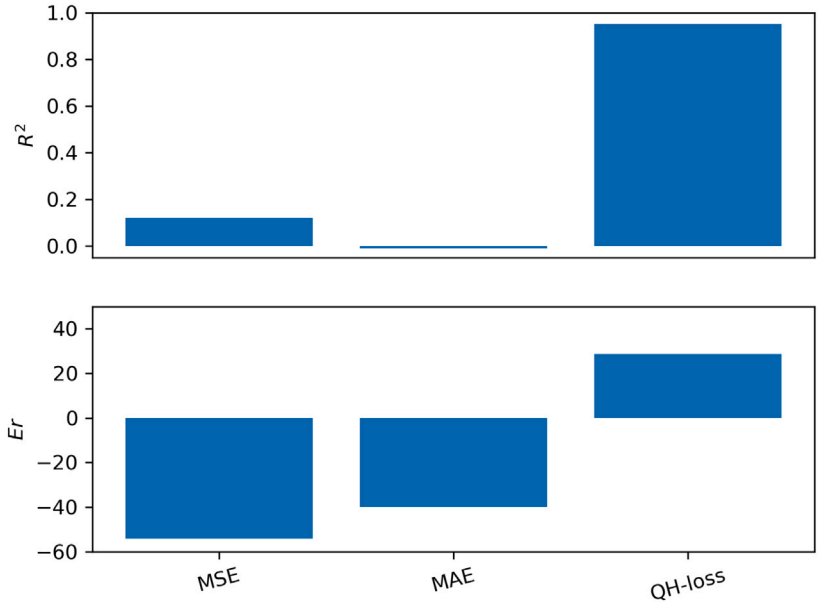

Fig. 12. Comparison with different loss function.

Table 6
RUL prediction quantitative results by SADT for FC1 at 550 h.

t_{pred} = 550 h	Est RUL	Er	RMSE	MAE	R^2
Failure threshold: 3.5% of P_{init}	519	−10.6610	0.0455	0.0350	0.9751
Failure threshold: 4.0% of P_{init}	486	−3.6247	0.0390	0.0277	0.9817
Failure threshold: 4.5% of P_{init}	521	−11.0874	0.0490	0.0338	0.9711
Failure threshold: 5.0% of P_{init}	416	11.30	0.0699	0.0548	0.9412
Failure threshold: 5.5% of P_{init}	552	−17.6972	0.0738	0.0577	0.9344

those in Table 5, the average performance is better, suggesting that the model trained on the quasi-steady state dataset performs more effectively when trained under constant conditions. The visual analysis in Fig. 14 highlights the adaptability of the SADT model. The predicted SoH curves closely align with the true SoH trajectories across all examined thresholds, confirming that the model's predictions maintain both linearity and monotonicity, as expected with typical degradation patterns. The SADT model's ability to generalize successfully across different domains, as demonstrated by the consistent performance metrics and accurate SoH predictions, underscores its effectiveness for RUL prediction in diverse operating scenarios.

The results in Table 7 demonstrate that our SADT model consistently outperforms mainstream data-driven methods, including SVM, LSTM [29], Bi-GRU [30], and CNN-RNN [31], in predicting the HIs of PEMFCs across different domain settings ("Source: FC1 to Target: FC2" and "Source: FC2 to Target: FC1") at the 4.5% threshold. In both

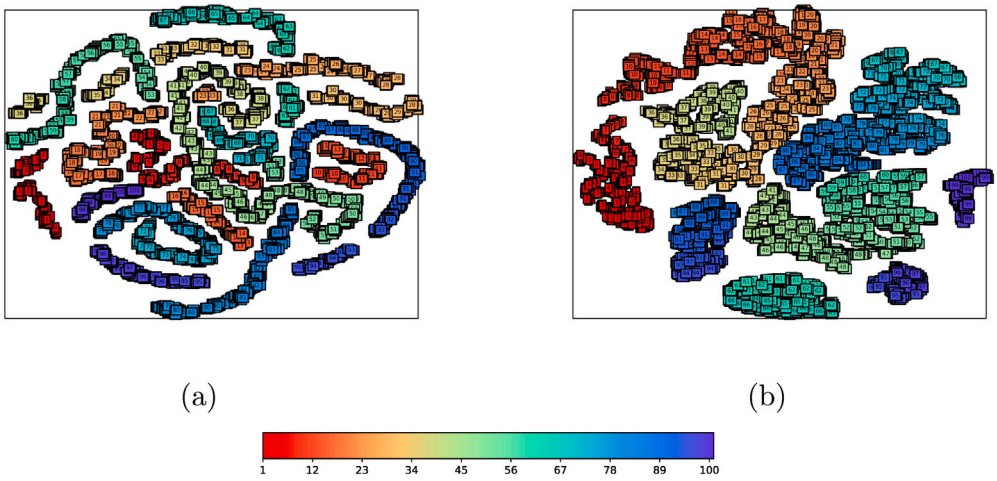

Fig. 13. Feature visualization results on the raw date of target domain: (a) before self-adaption; (b) after self-adaption.

Table 7
Comparative results with mainstream data-driven methods.

	$FC1 \rightarrow FC2$			$FC2 \rightarrow FC1$		
	$RMSE$	MAE	R^2	$RMSE$	MAE	R^2
SVM	0.1579	0.1237	0.5214	0.1377	0.1140	0.5491
LSTM [29]	0.1348	0.1056	0.6113	0.1335	0.1023	0.6223
Bi-GRU [30]	0.1309	0.0973	0.6238	0.1160	0.0747	0.6552
CNN-RNN [31]	0.0946	0.0699	0.7192	0.0890	0.0668	0.7321
SADT-no-DA	0.0779	0.0524	0.7825	0.0742	0.0496	0.8216
SADT	0.0640	0.0432	0.9508	0.0490	0.0338	0.9711

scenarios, our model achieves the lowest RMSE and MAE values, along with the highest R^2 values, indicating superior prediction accuracy and a better fit to actual degradation trends. The results also highlight that domain adaptation significantly enhances performance, as evidenced by an approximately 16% improvement over the SADT-no-DA model, which is the SADT method without the domain adaptation process.

6. Conclusion

In this paper, we present a self-adaptive digital twin framework enabled by transfer learning for predicting the RUL of PEMFCs under constant and quasi-steady state conditions. Our approach utilizes a deep CNN to achieve long-term predictions with SoH labeling. To enhance prediction accuracy, we introduced a novel QH-loss function, which is used to train the deep model with the SoH labels. Additionally, domain adaptation techniques have been employed to further improve accuracy and adaptability under both constant and quasi-steady state conditions. The primary conclusions are summarized as follows:

1. The experimental results confirm that the digital twin can accurately predict the RUL of PEMFC under both constant and quasi-steady state conditions, utilizing the designed uniform SoH labels. The average accuracy for the "Source: FC1 to Target: FC2" scenario is approximately 0.9411, while the average accuracy for the "Source: FC2 to Target: FC1" scenario is approximately 0.9607. These results indicate that our proposed methods are effective and robust across different scenarios.
2. The comparative experiment validated that the proposed method can accurately predict RUL throughout the entire degradation lifetime. The results demonstrate that, across different starting points, the overall accuracy consistently exceeds 0.85 throughout the entire period.
3. The comprehensive comparison results show that the SADT method performs superiorly compared to mainstream data-driven methods. Additionally, the results validate that domain adaptation enhances accuracy by approximately 16% compared to the SADT method without domain adaptation.

CRediT authorship contribution statement

Ming Zhang: Writing – review & editing, Writing – original draft, Visualization, Validation, Investigation, Data curation, Conceptualization. **Amirpiran Amiri:** Writing – review & editing, Validation, Supervision, Methodology, Investigation, Funding acquisition, Conceptualization. **Yuchun Xu:** Writing – review & editing, Supervision, Methodology, Investigation, Conceptualization. **Lucy Bastin:** Writing – review & editing, Validation, Methodology, Conceptualization. **Tony Clark:** Writing – review & editing, Validation, Supervision, Methodology, Investigation, Conceptualization.

Declaration of competing interest

The authors declare the following financial interests/personal relationships which may be considered as potential competing interests: Amirpiran Amiri reports financial support was provided by Engineering and Physical Sciences Research Council. Yuchun Xu reports financial support was provided by Innovate UK. If there are other authors, they declare that they have no known competing financial interests or personal relationships that could have appeared to influence the work reported in this paper.

Acknowledgments

This work was supported by Innovate UK project DIATOMIC (Digital InnovAtion TransfOrMatIve Change), UK with grant number 10055175. The authors would like to appreciate the financial support provided through EPSRC IAA 2022-23, UK Impact Builder Award.

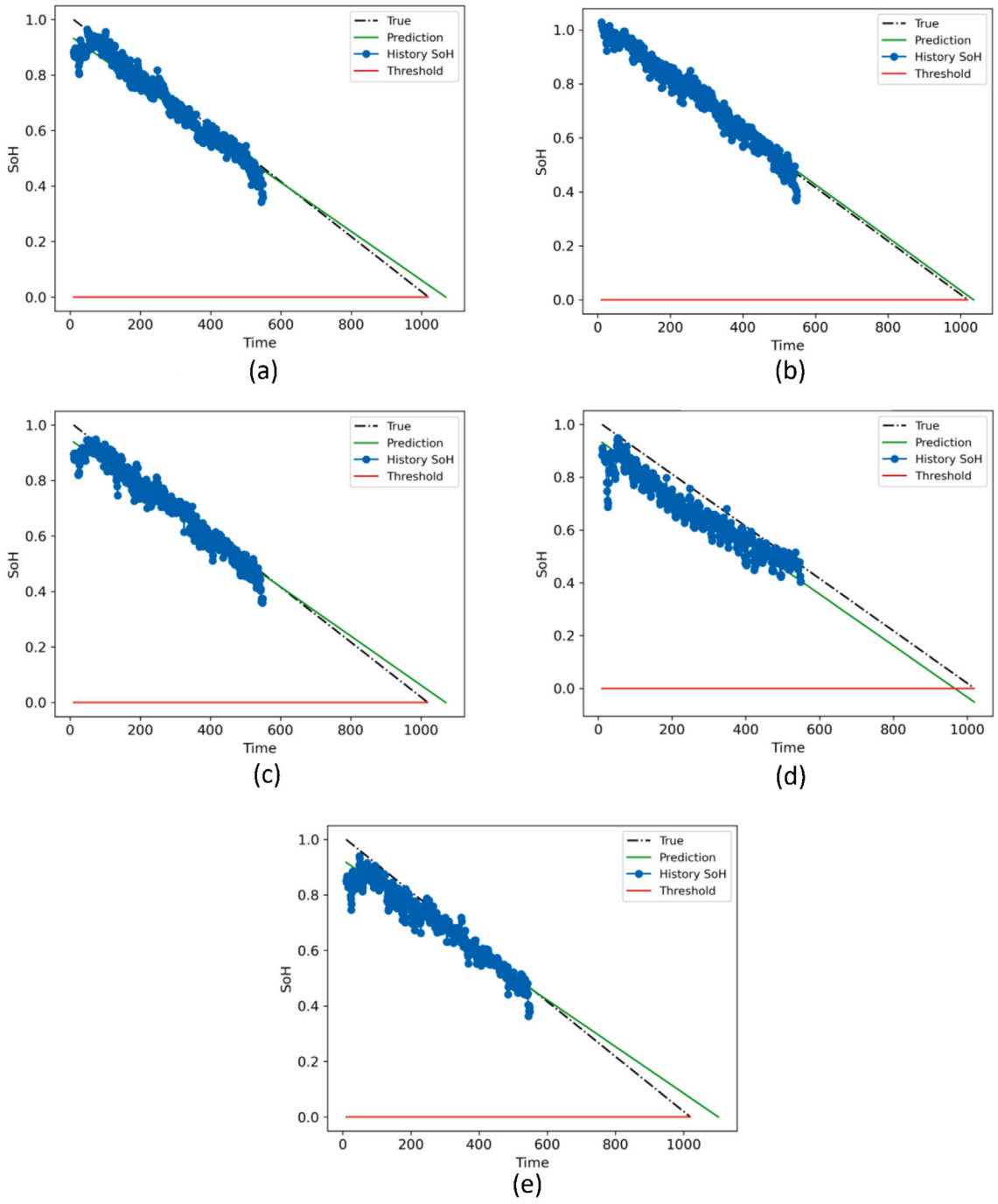

Fig. 14. RUL prediction results by SADT for FC1 at 550 h: (a) 3.5% of P_{init}, (b) 4.0% of P_{init}, (c) 4.5% of P_{init}, (d) 5.0% of P_{init}, (e) 5.5% of P_{init}.

References

[1] Ma R, Chai X, Geng R, Xu L, Xie R, Zhou Y, et al. Recent progress and challenges of multi-stack fuel cell systems: Fault detection and reconfiguration, energy management strategies, and applications. Energy Convers Manage 2023;285:117015.

[2] Kandidayeni M, Trovão J, Soleymani M, Boulon L. Towards health-aware energy management strategies in fuel cell hybrid electric vehicles: A review. Int J Hydrog Energy 2022;47(17):10021–43.

[3] Hua Z, Zheng Z, Pahon E, Péra M-C, Gao F. A review on lifetime prediction of proton exchange membrane fuel cells system. J Power Sources 2022;529:231256.

[4] Ming W, Sun P, Zhang Z, Qiu W, Du J, Li X, et al. A systematic review of machine learning methods applied to fuel cells in performance evaluation, durability prediction, and application monitoring. Int J Hydrog Energy 2023;48(13):5197–228.

[5] Jouin M, Gouriveau R, Hissel D, Péra M-C, Zerhouni N. Degradations analysis and aging modeling for health assessment and prognostics of PEMFC. Reliab Eng Syst Saf 2016;148:78–95.

[6] Kendall K, Ye S, Liu Z. The hydrogen fuel cell battery: Replacing the combustion engine in heavy vehicles. Engineering 2023;21:39–41.

[7] Yue M, Jemei S, Zerhouni N, Gouriveau R. Proton exchange membrane fuel cell system prognostics and decision-making: Current status and perspectives. Renew Energy 2021;179:2277–94.

[8] Achouch M, Dimitrova M, Ziane K, Sattarpanah Karganroudi S, Dhouib R, Ibrahim H, et al. On predictive maintenance in industry 4.0: Overview, models, and challenges. Appl Sci 2022;12(16):8081.

[9] Zhang M, Amaitik N, Wang Z, Xu Y, Maisuradze A, Peschl M, et al. Predictive maintenance for remanufacturing based on hybrid-driven remaining useful life prediction. Appl Sci 2022;12(7):3218.

[10] Ma Q, Zhang M, Xu Y, Song J, Zhang T. Remaining useful life estimation for turbofan engine with transformer-based deep architecture. In: 2021 26th

international conference on automation and computing. ICAC, IEEE; 2021, p. 1–6.
[11] Liu H, Chen J, Hissel D, Lu J, Hou M, Shao Z. Prognostics methods and degradation indexes of proton exchange membrane fuel cells: A review. Renew Sustain Energy Rev 2020;123:109721.
[12] Chen K, Laghrouche S, Djerdir A. Fuel cell health prognosis using unscented Kalman filter: Postal fuel cell electric vehicles case study. Int J Hydrog Energy 2019;44(3):1930–9.
[13] Ao Y, Laghrouche S, Depernet D, Chen K. Proton exchange membrane fuel cell prognosis based on frequency-domain Kalman filter. IEEE Trans Transp Electr 2021;7(4):2332–43.
[14] Zhang D, Cadet C, Yousfi-Steiner N, Bérenguer C. Proton exchange membrane fuel cell remaining useful life prognostics considering degradation recovery phenomena. Proc Inst Mech Eng O 2018;232(4):415–24.
[15] Wang P, Liu H, Chen J, Qin X, Lehnert W, Shao Z, et al. A novel degradation model of proton exchange membrane fuel cells for state of health estimation and prognostics. Int J Hydrog Energy 2021;46(61):31353–61.
[16] Liu H, Chen J, Hissel D, Su H. Remaining useful life estimation for proton exchange membrane fuel cells using a hybrid method. Appl Energy 2019;237:910–9.
[17] Ma R, Li Z, Breaz E, Liu C, Bai H, Briois P, et al. Data-fusion prognostics of proton exchange membrane fuel cell degradation. IEEE Trans Ind Appl 2019;55(4):4321–31.
[18] Ma R, Xie R, Xu L, Huangfu Y, Li Y. A hybrid prognostic method for PEMFC with aging parameter prediction. IEEE Trans Transp Electr 2021;7(4):2318–31.
[19] Zuo J, Lv H, Zhou D, Xue Q, Jin L, Zhou W, et al. Deep learning based prognostic framework towards proton exchange membrane fuel cell for automotive application. Appl Energy 2021;281:115937.
[20] Yue M, Li Z, Roche R, Jemei S, Zerhouni N. Degradation identification and prognostics of proton exchange membrane fuel cell under dynamic load. Control Eng Pract 2022;118:104959.
[21] Wang C, Li Z, Outbib R, Dou M, Zhao D. Symbolic deep learning based prognostics for dynamic operating proton exchange membrane fuel cells. Appl Energy 2022;305:117918.
[22] Zhu L, Chen J. Prognostics of PEM fuel cells based on Gaussian process state space models. Energy 2018;149:63–73.
[23] Deng H, Hu W, Cao D, Chen W, Huang Q, Chen Z, et al. Degradation trajectories prognosis for PEM fuel cell systems based on Gaussian process regression. Energy 2022;244:122569.
[24] Vichard L, Harel F, Ravey A, Venet P, Hissel D. Degradation prediction of PEM fuel cell based on artificial intelligence. Int J Hydrog Energy 2020;45(29):14953–63.
[25] Hua Z, Zheng Z, Péra M-C, Gao F. Data-driven prognostics for PEMFC systems by different echo state network prediction structures. In: 2020 IEEE transportation electrification conference & expo. ITEC, IEEE; 2020, p. 495–500.
[26] He K, Mao L, Yu J, Huang W, He Q, Jackson L. Long-term performance prediction of PEMFC based on LASSO-ESN. IEEE Trans Instrum Meas 2021;70:1–11.
[27] Hua Z, Zheng Z, Péra M-C, Gao F. Remaining useful life prediction of PEMFC systems based on the multi-input echo state network. Appl Energy 2020;265:114791.
[28] Hua Z, Zheng Z, Pahon E, Péra M-C, Gao F. Remaining useful life prediction of PEMFC systems under dynamic operating conditions. Energy Convers Manage 2021;231:113825.
[29] Wang C, Li Z, Outbib R, Dou M, Zhao D. A novel long short-term memory networks-based data-driven prognostic strategy for proton exchange membrane fuel cells. Int J Hydrog Energy 2022;47(18):10395–408.
[30] Zhang R, Chen T, Xiao F, Luo J. Bi-directional gated recurrent unit recurrent neural networks for failure prognosis of proton exchange membrane fuel cells. Int J Hydrog Energy 2022;47(77):33027–38.
[31] Wilberforce T, Alaswad A, Garcia-Perez A, Xu Y, Ma X, Panchev C. Remaining useful life prediction for proton exchange membrane fuel cells using combined convolutional neural network and recurrent neural network. Int J Hydrog Energy 2023;48(1):291–303.
[32] Chen K, Laghrouche S, Djerdir A. Aging prognosis model of proton exchange membrane fuel cell in different operating conditions. Int J Hydrog Energy 2020;45(20):11761–72.
[33] Yang J, Wang L, Zhang B, Zhang H, Wu X, Xu X, et al. Remaining useful life prediction of vehicle-oriented PEMFC systems based on IGWO-BP neural network under real-world traffic conditions. Energy 2024;291:130334.
[34] Mezzi R, Yousfi-Steiner N, Péra MC, Hissel D, Larger L. An echo state network for fuel cell lifetime prediction under a dynamic micro-cogeneration load profile. Appl Energy 2021;283:116297.
[35] Hua Z, Zheng Z, Pahon E, Péra M-C, Gao F. Lifespan prediction for proton exchange membrane fuel cells based on wavelet transform and echo state network. IEEE Trans Transp Electr 2021;8(1):420–31.
[36] Harel F. Ieee phm data challenge 2014, fclab. 2021, http://dx.doi.org/10.25666/DATAUBFC-2021-07-19.
[37] Krizhevsky A, Sutskever I, Hinton GE. Imagenet classification with deep convolutional neural networks. In: Advances in neural information processing systems. 2012, p. 1097–105.
[38] Simonyan K, Zisserman A. Very deep convolutional networks for large-scale image recognition. 2014, arXiv preprint arXiv:1409.1556.
[39] He K, Zhang X, Ren S, Sun J. Deep residual learning for image recognition. In: Proceedings of the IEEE conference on computer vision and pattern recognition. 2016, p. 770–8.
[40] LeCun Y, Bengio Y, Hinton G. Deep learning. Nature 2015;521(7553):436.
[41] Long M, Cao Y, Wang J, Jordan M. Learning transferable features with deep adaptation networks. In: International conference on machine learning. PMLR; 2015, p. 97–105.
[42] Zhang Y, Zhang M, Liu C, Feng Z, Xu Y. Reliability enhancement of state of health assessment model of lithium-ion battery considering the uncertainty with quantile distribution of deep features. Reliab Eng Syst Saf 2024;110002.
[43] Li X, Ding Q, Sun J-Q. Remaining useful life estimation in prognostics using deep convolution neural networks. Reliab Eng Syst Saf 2018;172:1–11.
[44] Zhang M, Wang D, Lu W, Yang J, Li Z, Liang B. A deep transfer model with wasserstein distance guided multi-adversarial networks for bearing fault diagnosis under different working conditions. IEEE Access 2019;7:65303–18.
[45] Van der Maaten L, Hinton G. Visualizing data using t-SNE. J Mach Learn Res 2008;9(11).